Conference on Modelling Fluid Flow (CMFF'18)
The 17th International Conference on Fluid Flow Technologies
Budapest, Hungary, September 4-7, 2018

COMPUTATIONS OF NON-ISOTHERMAL COMPRESSIBLE GAS FLOWS AROUND MOVING SOLID OBJECT

Daisuke Toriu[1], Satoru Ushijima[2]

[1] Corresponding Author. Academic Center for Computing and Media Studies (ACCMS), Kyoto University. Yoshida Honmachi, Sakyo-ku, Kyoto, 606-8501, Japan. E-mail: toriu.daisuke.8v@kyoto-u.ac.jp
[2] Academic Center for Computing and Media Studies (ACCMS), Kyoto University. Yoshida Honmachi, Sakyo-ku, Kyoto, 606-8501, Japan. E-mail: ushijima.satoru.3c@kyoto-u.ac.jp

ABSTRACT

In this study, we applied a computational method for non-isothermal compressible flows around moving solid objects based on the mixture model to heat transfer around a rotating triangular solid object. In our proposed method, cell-averaged governing equations for multiphase fields consisting of compressible gas and solid objects are solved by a computational method for compressible low Mach number flows. Thus, the proposed method enables to calculate non-isothermal compressible gas flows around moving solid objects on an orthogonal grid system. As a result of the computation, it was demonstrated that the proposed method enables to predict the heat transfer around the rotating triangular solid object while considering the physical properties of the solid body appropriately. In addition, the obtained maximum rate of the gas density change was about 17% when gas flows and convective heat transfer are fully developed around the solid object. From this result, it was confirmed that variations of the gas density are non-negligible in this application.

Keywords: fluid-solid thermal interaction, mixture model, moving solid object, non-isothermal compressible flow

NOMENCLATURE

a	$[m/s]$	speed of sound
C_P, C_V	$[J/(kg \cdot K)]$	specific heat at constant pressure and volume
e	$[J/kg]$	internal energy
f_i	$[m/s^2]$	acceleration of external force
g	$[m/s^2]$	gravitational acceleration
p	$[Pa]$	pressure
q_i	$[W/m^2]$	heat flux component
T	$[K]$	temperature
t	$[s]$	time
u_i	$[m/s]$	velocity component
x_i	$[m]$	orthogonal coordinate component
β	$[1/K]$	coefficient of thermal expansion
γ	[-]	specific heat ratio
ΔT	$[K]$	characteristic temperature difference
Δt	$[s]$	time increment
Δx_i	$[m]$	cell size in x_i direction
δ_{ij}	[-]	Kronecker's delta
λ	$[W/(m \cdot K)]$	thermal conductivity
μ	$[Pa \cdot s]$	coefficient of viscosity
ρ	$[kg/m^3]$	density
σ_{ij}	$[Pa]$	stress
τ_{ij}	$[Pa]$	viscous stress
ϕ_k	[-]	volume fraction of phase k

Subscripts and Superscripts

$f1$	fluid 1
$f2$	fluid 2
f	fluid 1 and 2
s	solid
0	value at initial condition
$'$	non-dimensional value

1. INTRODUCTION

Thermal interactions between fluids and moving solid objects are important phenomena in engineering and many numerical studies have been conducted [1, 2, 3]. However, most of the previous studies were based on the fluid incompressibility assumption and little study has been done to the problems in which variations of fluid density due to temperature and pressure differences are non-negligible.

Against the aforementioned background, we proposed a new computational method for non-isothermal compressible flows around solid objects based on the mixture model [4, 5]. In our proposed method, cell-averaged governing equations for multiphase fields are solved by the computational method for non-isothermal compressible flows, which can be applied to low Mach number flows by adapting the implicit time integration in pressure calculations to improve the Courant-Friedrichs-Lewy (CFL) condition based on the speed of sound. Since the cell-averaged governing equations are derived based on the mixture model, the proposed method enables to calculate thermal interactions between compressible gas and solid objects without setting the adaptive grid to phase boundaries. The proposed method was applied to the heat transfer around stationary solid objects and we confirmed that the reasonable temperature distributions are predicted through the comparisons with by previous experimental and numerical results [4, 5].

In this study, the proposed method is applied to the heat transfer around a rotating triangular solid in a square cavity. The central circular area of the triangular solid is heated at 400 K and all boundaries of the computational area are cooled at 300 K. Thus, it is expected that variations of gas density due to the temperature difference are non-negligible when the gas flow and convective heat transfer are fully developed around the solid object. In addition, two different physical properties of the solid are considered in this study. For the case 1, density, specific heat, and thermal conductivity of the solid are set equal to those of the gas. By contrast, physical properties of iron (Fe) are considered in the case 2. The influence of such differences in physical properties is discussed through comparisons of predicted results.

2. NUMERICAL METHOD

2.1. Governing equations for multiphase field

In this study, a multiphase field consisting of an ideal gas and moving solid objects (rigid body) is treated as a one-fluid that has uniform physical properties. Hereinafter, the ideal gas around the solid object is referred to as a "fluid 1". By contrast, the solid area is assumed to be a "fluid 2" that has physical properties of the fluid 1 as shown in Figure 1. In addition, temperature and velocity of the fluid 2 are same value as those of the solid. Based on this assumption, phase-averaged governing equations for

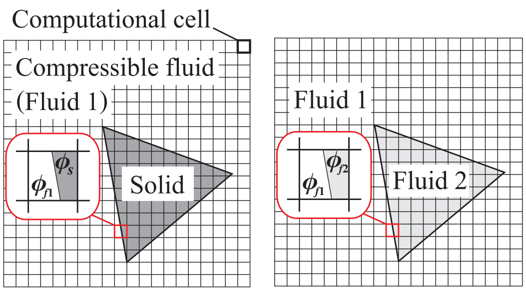

Figure 1. Multiphase fields considered in this study and definitions of ϕ_{f1}, ϕ_{f2}, and ϕ_s

the multiphase field consisting of two immiscible fluids are derived based on the mixture model [6]. We adopt the orthogonal grid system in this study and governing equations for the one-fluid (referred to hereinafter as a "phase-averaged mixture") are derived based on the volume fractions of phases, ϕ_{f1} and ϕ_{f2}, in each computational cell as shown in Figure 1 to easily treat moving solid boundaries.

Derived governing equations for the multiphase field are solved by a computational method for non-isothermal compressible flows that enables to calculate low Mach number flows free from the CFL condition based on the speed of sound [4]. In addition, we adopt averaging methods for momentums of the phase-averaged mixture and the heat conduction equation considering the physical properties of solid objects in suitable computational stages to accurately estimate effects of the solid phase on flow and temperature fields.

The phase-averaged governing equations for the fluid 1 and 2 are given by the following mass, momentum, and energy equations:

$$\frac{\partial \rho}{\partial t} + \frac{\partial (\rho u_i)}{\partial x_i} = 0 \tag{1}$$

$$\frac{\partial (\rho u_i)}{\partial t} + \frac{\partial (\rho u_i u_j)}{\partial x_j} = \frac{\partial \sigma_{ij}}{\partial x_j} + \rho f_i + M_i \tag{2}$$

$$\frac{\partial (\rho e)}{\partial t} + \frac{\partial (\rho e u_j)}{\partial x_j} = \sigma_{ij}\frac{\partial u_i}{\partial x_j} + E - M_i u_i \tag{3}$$

where ρ, u_i, σ_{ij}, and e are density, velocity, stress, and internal energy of the phase-averaged mixture consisting of the fluid 1 and 2, respectively. In addition, M_i is the mixture momentum source due to surface tension and E is the mixture total energy source from interfaces [6]. In this study, we assume the effects of these terms to be negligible compared with other terms ($M_i \approx 0$ and $E \approx 0$). Actually, it was confirmed that the reasonable results can be obtain with the above assumption for M_i and E through the application to the experiment on the natural convection around a horizontal circular cylinder [5]. As given by Eq. (3), a heat flux term is not considered in the energy equation for the phase-averaged mixture consisting of the fluid 1 and 2 since heat conduction is estimated in a computational stage for the phase-averaged mixture consisting of the fluid 1 and the solid.

Phase-averaged variables ρ, u_i, σ_{ij}, and e are defined as

$$\rho = \sum_k \phi_k \rho_k \tag{4}$$

$$u_i = \frac{1}{\rho}\sum_k \phi_k \rho_k u_{k,i} \tag{5}$$

$$\sigma_{ij} = \sum_k (\phi_k \sigma_{k,ij} - \phi_k \rho_k w_{k,i} w_{k,j}) \tag{6}$$

$$e = \frac{1}{\rho}\sum_k \left(\phi_k\rho_k e_k + \frac{1}{2}\phi_k\rho_k w_{k,i}^2\right) \quad (7)$$

where $k = f1, f2$ and $w_{k,i}$ is defined as $w_{k,i} \equiv u_{k,i} - u_i$. Subscripts $f1$ and $f2$ represent the fluid 1 and 2, namely ρ_{f1} represents the density of the fluid 1. In addition, we assume that $w_{k,i}$ is negligible ($w_{k,i} \approx 0$) by setting fine computational cells for the solid size. Consequently, Eqs. (6) and (7) are simplified as

$$\sigma_{ij} = \sum_k \phi_k\sigma_{k,ij} \quad (8)$$

$$e = \frac{1}{\rho}\sum_k \rho_k e_k \quad (9)$$

In this study, we also assume that differences between T_{f1} and T_{f2} $(= T_s)$ in all computational cells are sufficiently small ($T_{f1} \approx T_{f2}$ $(= T_s)$) by setting fine computational cells for the solid size. On the basis of this assumption, the relationship between e and T is approximately given by

$$\begin{aligned} e &= \frac{1}{\rho}\sum_k \phi_k\rho_k C_{V,k}T_k = \frac{1}{\rho}C_{V,f}\sum_k \phi_k\rho_k T_k \\ &\approx \frac{1}{\rho}C_{V,f}T\sum_k \phi_k\rho_k = C_{V,f}T \end{aligned} \quad (10)$$

where $k = f1, f2$. In addition, $C_{V,f}$ represents uniformly the specific heat at constant volume of the fluid 1 and 2 because of the assumption that $C_{V,f2}$ is equal to $C_{V,f1}$. The stress of the phase-averaged mixture consisting of the fluid 1 and 2 is approximately estimated as follows [4]:

$$\begin{aligned} \sigma_{ij} &= -\sum_k \phi_k p_k\delta_{ij} + \sum_k \phi_k\tau_{k,ij} \\ &= -p\delta_{ij} + \sum_k \phi_k\tau_{k,ij} \approx -p\delta_{ij} + \tau_{ij} \end{aligned} \quad (11)$$

where $k = f1, f2$ and p is defined as $p = \sum_k \phi_k p_k$. Herein, we use the following approximation for τ_{ij} to estimate σ_{ij} simply from u_i [4]:

$$\begin{aligned} \tau_{ij} &= \sum_k \phi_k\left\{\mu_k\left(\frac{\partial u_{k,i}}{\partial x_j} + \frac{\partial u_{k,j}}{\partial x_i}\right) - \frac{2}{3}\mu_k\frac{\partial u_{k,m}}{\partial x_m}\delta_{ij}\right\} \\ &\approx \mu_f\left(\frac{\partial u_i}{\partial x_j} + \frac{\partial u_j}{\partial x_i}\right) - \frac{2}{3}\mu_f\frac{\partial u_m}{\partial x_m}\delta_{ij} \end{aligned} \quad (12)$$

where $k = f1, f2$.

The equation of state for the phase-averaged mixture consisting of the fluid 1 and 2 is derived as follows based on the assumption that physical properties of the two fluids are uniform and $T_{f1} \approx T_{f2}$:

$$\begin{aligned} p &= \sum_k \phi_k p_k = \sum_k \phi_k\rho_k(\gamma_k - 1)C_{V,k}T_k \\ &\approx (\gamma_f - 1)C_{V,f}T\sum_k \phi_k\rho_k \\ &= \rho(\gamma_f - 1)C_{V,f}T \end{aligned} \quad (13)$$

where $k = f1, f2$.

The heat conduction is estimated in the computational stage for the phase-averaged mixture consisting of the fluid 1 and the solid. The heat conduction equation on this stage is given by

$$\frac{\partial(\rho C_V)_m T}{\partial t} = -\frac{\partial q_{m,j}}{\partial x_j} \quad (14)$$

The subscript m represents the phase-averaged mixture consisting of the fluid 1 and the solid. Here, $(\rho C_V)_m$ is given by

$$(\rho C_V)_m = \sum_k \phi_k\rho_k C_{V,k} \quad (15)$$

where $k = f1, s$. In addition, s represents the solid phase. The heat flux $q_{m,i}$ is estimated as follows based on the assumption that $T_{f1} \approx T_{f2}$ $(= T_s)$:

$$\begin{aligned} q_{m,i} &= \sum_k \phi_k q_{k,j} = -\sum_k \phi_k\lambda_k\frac{\partial T_k}{\partial x_i} \\ &\approx -\left(\sum_k \phi_k\lambda_k\right)\frac{\partial T}{\partial x_j} = -\lambda_m\frac{\partial T}{\partial x_j} \end{aligned} \quad (16)$$

where $k = f1, s$ and λ_m is given by

$$\lambda_m = \sum_k \phi_k\lambda_k \quad (17)$$

In this study, Eqs. (1), (2), (3), and (14) are solved by a numerical algorithm for compressible low Mach number flows [4, 5].

2.2. Numerical procedure

The numerical procedure of the proposed method is divided into advection, diffusion, and acoustic stages [4]. Hereinafter, variables updated in these stages are represented as Q^*, Q^{**}, and Q^{n+1}, respectively. Discretizations of the Eqs. (1), (2), (3), and (14) are conducted on an orthogonal collocated grid system based on the finite volume method (FVM). In the advection and diffusion stages, Euler method is adopted and variations of variables due to the advection and diffusion terms are estimated explicitly. By contrast, the pressure at the next time step is calculated by implicit time integration in the acoustic stage to adopt a large time increment for compressible low Mach number flows free from the CFL condition based on the speed of sound.

In the advection stage, we explicitly solve advection equations for the phase-averaged mixture consisting of the fluid 1 and 2 as follows:

$$\frac{\rho^* - \rho^n}{\Delta t} + \frac{\partial(\rho^n u_j^n)}{\partial x_j} = 0 \quad (18)$$

$$\frac{(\rho u_i)^* - (\rho u_i)^n}{\Delta t} + \frac{\partial\{(\rho u_i)^n u_j^n\}}{\partial x_j} = 0 \quad (19)$$

$$\frac{(\rho e)^* - (\rho e)^n}{\Delta t} + \frac{\partial\{(\rho e)^n u_j^n\}}{\partial x_j} = 0 \quad (20)$$

The advection terms are discretized with the FVM and the third order MUSCL-TVD scheme [7]. Therefore, mass conservation is satisfied sufficiently in the proposed method.

To consider effects of moving solid objects on flow fields, we conduct the following averaging operation for momentums:

$$u_i^* = \frac{1}{\rho_m^*}\left[\phi_{f1}^n(\rho u_i)^* + \phi_s^n(\rho u_i)_s\right] \tag{21}$$

where ρ_m is given by

$$\rho_m^* = \phi_{f1}\rho^* + \phi_s\rho_s \tag{22}$$

We conduct the same averaging operations for the momentums in the following diffusion and acoustic stages.

In the diffusion stage, the momentums and the pressure are calculated on the basis of the governing equations for the phase-averaged mixture consisting of the fluid 1 and 2. By contrast, the calculation of the temperature is divided into two steps. In the first step, the tentative temperature T' is calculated on the basis of the governing equations for the phase-averaged mixture consisting of the fluid 1 and 2. In the second step, we obtain T^{**} from T' using the heat conduction equation (14) as shown in Figure 2 to consider effects of the solid object on temperature fields appropriately.

The governing equations in the diffusion stage are given as follows for the phase-averaged mixture consisting of the fluid 1 and 2:

$$\frac{\rho^{**} - \rho^*}{\Delta t} = 0 \tag{23}$$

$$\frac{(\rho u_i)^{**} - (\rho u_i)^*}{\Delta t} = \frac{\partial \tau_{ij}^*}{\partial x_j} \tag{24}$$

$$\frac{(\rho e)^{**} - (\rho e)^*}{\Delta t} = \tau_{ij}^*\frac{\partial u_i^*}{\partial x_j} \tag{25}$$

From Eqs. (24) and (25), u_i^{**} and T' are estimated as follows:

$$\frac{u_i^{**} - u_i^*}{\Delta t} = \frac{1}{\rho^*}\frac{\partial \tau_{ij}^*}{\partial x_j} \tag{26}$$

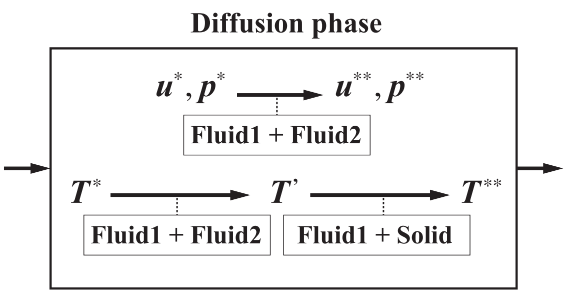

Figure 2. Updating method for variables in diffusion stage [4]

$$\frac{T' - T^*}{\Delta t} = \frac{1}{\rho^* C_{V,f}}\left\{\frac{\partial(\tau_{ij}^* u_i^*)}{\partial x_j} - \frac{\rho^*(u_i^{**2} - u_i^{*2})}{2\Delta t}\right\} \tag{27}$$

To consider effects of the solid object on temperature fields, T^{**} is estimated on the basis of the heat conduction equations for the phase-averaged mixture consisting of the fluid 1 and the solid as follows:

$$\frac{T^{**} - T'}{\Delta t} = \frac{1}{(\rho C_V)_m^*}\frac{\partial}{\partial x_j}\left(\lambda_m \frac{\partial T^{**}}{\partial x_j}\right) \tag{28}$$

On the right-hand side of Eq. (28), $(\rho C_V)_m^*$ and λ_m are given by

$$(\rho C_V)_m^* = \phi_{f1}^n \rho_{f1}^* C_{V,f1} + \phi_s^n \rho_s C_{V,s} \tag{29}$$

$$\lambda_m = \sum_k \phi_k^n \lambda_k \tag{30}$$

where $k = f1, s$ and ρ_{f1}^* is estimated by

$$\rho_{f1}^* = \frac{\rho^* - \phi_{f2}^n \rho_{f2}}{\phi_{f1}^n} \tag{31}$$

When the computational area contains isothermal solid objects, T^{**} is calculated by the following equation instead of by Eq. (28):

$$\frac{T^{**} - T'}{\Delta t} = (1 - \phi_{sc}^n)\Theta + \phi_{sc}^n T_{sc} \tag{32}$$

where Θ is the right-hand side of Eq. (28) and the subscript sc represents the isothermal solid object.

Pressure changes of the fluid 1 and 2 in the diffusion stage are given as follows [8]:

$$p_k^{**} - p_k^* = \frac{\gamma_k - 1}{\gamma_k}\frac{\rho_k^* C_{P,k}}{\rho_k^* C_{P,k}\mu_{J,k} + 1}(T_k^{**} - T_k^*) \tag{33}$$

where $k = f1, f2$. As mentioned above, p is defined as the volume-averaged variable. Thus, the pressure change in the diffusion stage is given by the assumptions that physical properties of the fluid 1 and 2 are uniform and $T_{f1}^{**} \approx T_{f2}^{**} (= T_s^{**})$ as follows:

$$\begin{aligned} p^{**} - p^* &\approx \frac{\gamma_f - 1}{\gamma_f}\left(\sum_k \phi_k^n \rho_k^*\right) C_{P,f}(T^{**} - T^*) \\ &= \frac{\gamma_f - 1}{\gamma_f}\rho^* C_{P,f}(T^{**} - T^*) \end{aligned} \tag{34}$$

where $k = f1, f2$ and $\mu_{J,k} = 0$ in ideal gas.

In the acoustic stage, the variations of variables due to pressure and external force are represented as

$$\frac{\rho^{n+1} - \rho^{**}}{\Delta t} = 0 \tag{35}$$

$$\frac{(\rho u_i)^{n+1} - (\rho u_i)^{**}}{\Delta t} = -\frac{\partial p^{n+1}}{\partial x_i} + \rho^{**} f_i \tag{36}$$

$$\frac{(\rho e)^{n+1} - (\rho e)^{**}}{\Delta t} = -p^{n+1}\frac{\partial u_i^{n+1}}{\partial x_i} \tag{37}$$

From Eqs. (35) ~ (37) and (13), the pressure equation in acoustic stage is derived as follows:

$$\frac{1}{\rho^{**}a^2}\frac{p^{n+1}-p^{**}}{\Delta t} = -\frac{\partial}{\partial x_i}\left(-\frac{1}{\rho^{**}}\frac{\partial p^{n+1}}{\partial x_i}\Delta t + u_i^{**}\right) + \frac{1}{\gamma_f}\frac{\partial u_i^{**}}{\partial x_i} \quad (38)$$

where $a^{**} = \sqrt{(\gamma_f p^{**})/\rho^{*}}$. In addition, u_i^{n+1} and e^{n+1} are calculated from Eqs. (36) and (37) with obtained p^{n+1}, respectively. As given by Eq. (38), the pressure is calculated implicitly in our proposed method. Thus, the proposed method enables us to adopt a large time increment for compressible low Mach number flows free from the CFL condition based on the speed of sound [4].

3. RESULTS AND DISCUSSION

We conducted numerical experiments on heat transfer around a rotating triangular solid in a square cavity to discuss the applicability of the proposed method. The proposed numerical model was implemented within our in-house solver and computations were conducted on the supercomputer system of Kyoto University (CRAY CS400 2820XT, Intel Xeon Broadwell 18cores 2.1GHz x 2 / node) using the domain decomposition method with the Message Passing Interface (MPI).

Figure 3 shows computational area containing a rotating triangular solid object. The lengths L and r_t are 5.0×10^{-2} m and $L/3$, respectively. The central circular area ($r_h = 3L/40$) of the triangular solid object is heated at 400 K and all boundaries of the computational area are cooled at 300 K. In this numerical experiment, $\beta\Delta T$ is about 0.33. This shows that the variations of the gas density are non-negligible when the gas flow and the heat transfer are fully developed around the solid object. As shown in Figure 3, the triangular solid object rotates in the clockwise direction

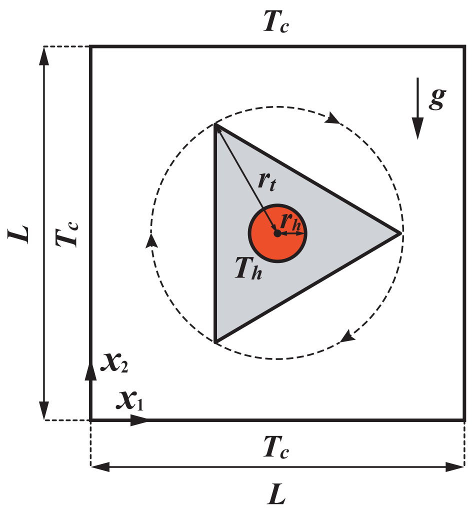

Figure 3. Computational area containing rotating triangular solid object [4]

Table 1. Physical properties of solid object

	Case 1	Case 2
ρ_s $[kg/m^3]$	1.17	7.87×10^3
λ_s $[W/(m \cdot K)]$	2.50×10^{-2}	80.3
$C_{V,s}$ $[J/(kg \cdot K)]$	4.20×10^3	4.42×10^3

at the angular velocity ω. Herein, ω is given by

$$\omega = \frac{t}{t_b}\pi \quad (0 \le t \le t_b) \quad (39)$$

$$\omega = \pi \quad (t_b < t) \quad (40)$$

where t_b is 3.0 s in this study.

The fluid is an ideal gas and the specific heat ratio γ_f of the fluid is 1.40. As initial conditions, temperature T_0 of the fluid and the Prandtl number Pr are 300 K and 0.70, respectively. In this application, we take two different values of physical properties of the solid object as given in Table 1. In the case 1, physical properties of the solid object are those of the fluid in the initial state. By contrast, we assume the solid object to be iron (Fe) in the case 2 to confirm that the proposed method enables to estimate the effect of the physical properties on flow fields and temperature distributions reasonably.

The number of computational cells is 150×150 for the case 1 and 2. In the proposed method, it is necessary to set the fine computational cells for the solid object to obtain reasonable results. Hence, we conducted the several computations under the different cell size conditions and compared predicted Nusselt numbers on the wall boundaries with each other. As a result, it was confirmed that 150×150 cells are sufficiently fine for this numerical experiment. In addition, the time increment Δt is 1.50×10^{-4} s and 1.00×10^{-4} s for the case 1 and 2, respectively. Under these conditions for Δt, the obtained maximum Courant numbers $C_{a,\max}$ based on the speed of sound in the case 1 and 2 were 1.68×10^2 and 1.21×10^2. Herein, C_a is given by

$$C_a = \max\left\{\frac{|u_1| + a}{\Delta x_1}\Delta t, \; \frac{|u_2| + a}{\Delta x_2}\Delta t\right\} \quad (41)$$

Figures 4 and 5 show time histories of isotherms (the isotherm interval is $\Delta T/10$). Herein, t' is the non-dimensional time defined as $t' \equiv t/(2\pi/\omega_{\max})$. In this study, $\omega_{\max}$ is π rad/s as given by Eqs. (39) and (40). Initially, temperature is changed concentrically in the solid object as shown in Figures 4 (a) and 5 (a). After that, the fluid around the solid object is heated and the convective heat transfer occurs. As shown in Figures 4 (d) and 5 (d), thermal boundary layers around the solid object become thin in the case 2 since λ_s in the case 2 is about 3,000 times larger than that in the case 1 and larger temperature differences occur between the solid surface and wall boundaries of the computational area.

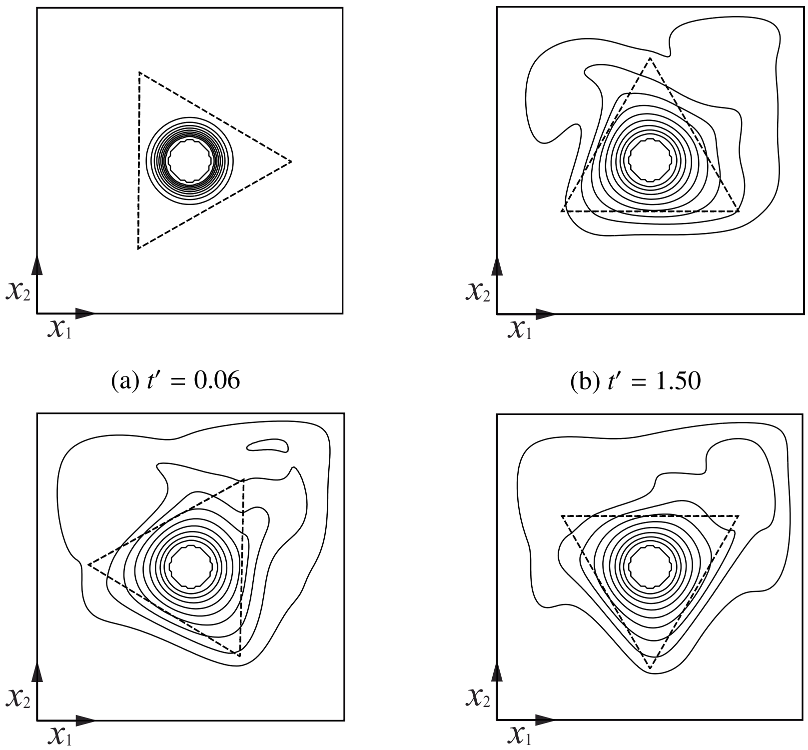

(a) $t' = 0.06$ (b) $t' = 1.50$

(c) $t' = 4.92$ (d) $t' = 6.00$

Figure 4. Time history of isotherms predicted in case 1 (isotherm interval is $\Delta T/10$)

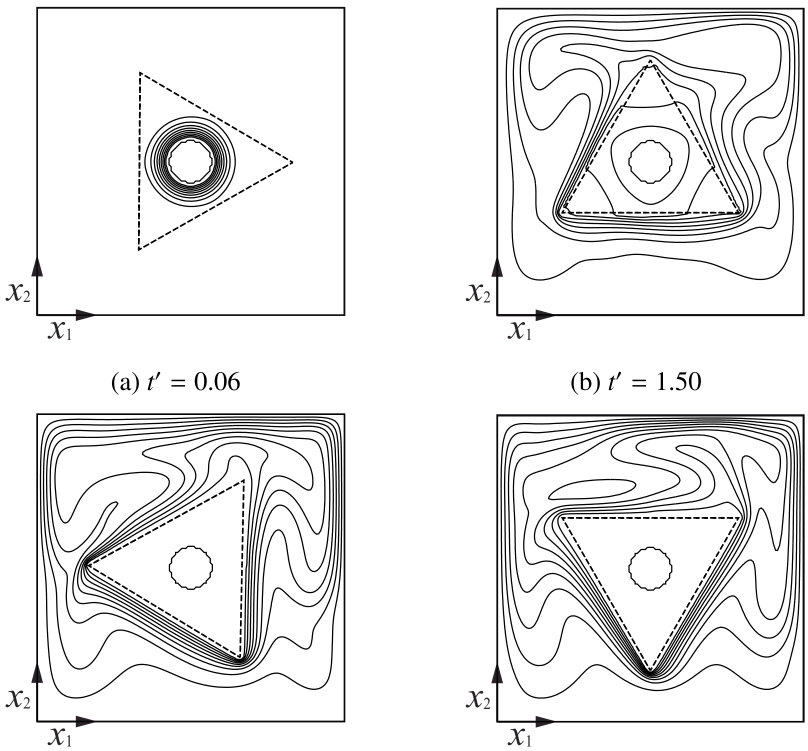

(a) $t' = 0.06$ (b) $t' = 1.50$

(c) $t' = 4.92$ (d) $t' = 6.00$

Figure 5. Time history of isotherms predicted in case 2 (isotherm interval is $\Delta T/10$)

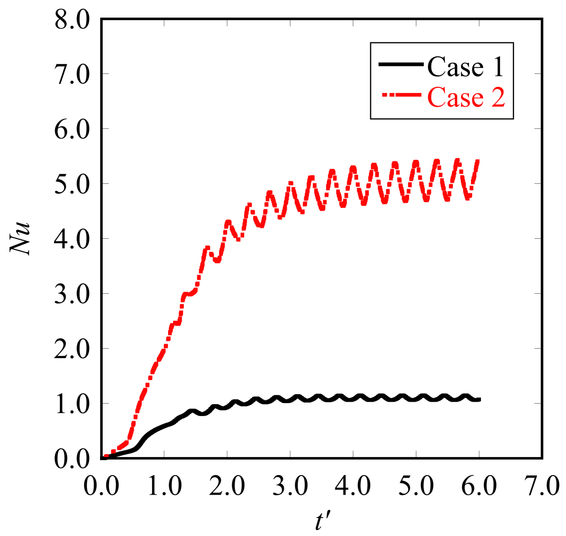

Figure 6. Time history of Nu predicted in case 1 and 2

Figure 6 shows the time history of the averaged Nusselt number Nu on the square wall boundary. Here, Nu is given by

$$Nu = \frac{Nu_w + Nu_e + Nu_s + Nu_n}{4} \tag{42}$$

where Nu_w, Nu_e, Nu_s, and Nu_n are averaged Nusselt numbers on the walls at $x_1 = 0$, $x_1 = L$, $x_2 = 0$, and $x_2 = L$, respectively. For example, Nu_w is given by

$$Nu_w = -\int_0^1 \left.\frac{\partial \theta}{\partial X_1}\right|_{X_1=0} dX_2 \tag{43}$$

where θ and X_i $(i = 1, 2)$ are the non-dimensional temperature and the non-dimensional coordinate component defined as $\theta \equiv (T - T_c)/(T_h - T_c)$ and $X_i \equiv x_i/L$. As shown in Figure 6, we can see periodic oscillations of Nu due to counterclockwise convection rolls that occur around vertexes of the rotating triangular solid object (Figure 4 (d) and 5 (d)). In addition, we obtained a reasonable result that Nu in the case 2 is lager than that in the case 1 since the more developed convective heat transfer occurs in the case 2. From the results obtained in this numerical experiment, we concluded that the proposed method enables to predict the heat transfer around the moving solid object considering the differences of the physical properties between solid and fluid phases on the orthogonal structured grid system.

Furthermore, we checked variations of the fluid density in two cases. As a result of the computation, the value of $\rho_{f,\min}/\rho_{f,0}$ was 0.901 and 0.826 in the case 1 and 2, respectively. Herein, $\rho_{f,\min}$ is the minimum fluid density in the computational cell that contains only fluid, and $\rho_{f,0}$ is the fluid density in the initial condition. These results show that variations of the fluid density are non-negligible and the consideration of the fluid compressibility is required to estimate high buoyancy flows occurred around the rotating triangular solid object.

4. CONCLUSION

In this study, we applied the proposed computational method for non-isothermal compressible flows around moving solid objects based on the mixture model to the heat transfer around a rotating triangular solid object in a square cavity. Since we use phase-averaged governing equations for multiphase fields and the computational method for compressible low Mach number flows adopting the implicit pressure calculation stage, the proposed method enables to calculate non-isothermal compressible gas flows around moving solid objects on the orthogonal grid system free from the CFL condition based on the speed of sound.

As a result of the computation, the reasonable temperature distributions and averaged Nusselt numbers were predicted while considering the physical properties and movements of the solid object. Furthermore, the maximum rate of the gas density change was about 17% in the case 2. This result indicates that variations of the gas density are non-negligible and the consideration of the fluid compressibility is required for this application. In our future works, the proposed method will be applied to the experimental results and its validity will be discussed.

ACKNOWLEDGEMENT

This work was supported by JSPS KAKENHI Grant Number JP16K17552.

REFERENCES

[1] Ghalambaz, M., Jamesahar, E., Ismael, M. A., and Chamkha, A. J., 2017, "Fluid-Structure Interaction Study of Natural Convection Heat transfer over a Flexible Oscillating Fin in a Square Cavity", *International Journal of Thermal Sciences*, Vol. 111, pp. 256–273.

[2] Ismael, M. A., and Jasim, H. F., 2018, "Role of the Fluid-Structure Interaction in Mixed Convection in a Vented Cavity", *International Journal of Mechanical Sciences*, Vol. 135, pp. 190–202.

[3] Gu, J., Takeuchi, S., and Kajishima, T., 2018, "Influence of Rayleigh Number and Solid Volume Fraction in Particledispersed Natural Convection", *International Journal of Heat and Mass Transfer*, Vol. 120, pp. 250–258.

[4] Toriu, D., and Ushijima, S., 2017, "Computational Method for Thermal Interactions between Compressible Fluid and Moving Solid Based on Mixture Model", *Journal of JSCE Ser A2 (Applied Mechanics)*, Vol. 73 (2), pp. I_143–I_152, (in Japanese).

[5] Toriu, D., and Ushijima, S., 2018, "Multiphase Computational Method for Thermal Interactions between Compressible Fluid and Arbitrarily Shaped Solids", *International Journal for Nu-*

merical Methods in Fluids, Vol. 87 (8), pp. 383–400.

[6] Ishii, M., and Hibiki, T., 2011, *Thermo-Fluid Dynamics of Two-Phase Flow*, Springer.

[7] Yamamoto, S., and Daiguji, S., 1993, "Higher-Order-Accurate Upwind Schemes for Solving the Compressible Euler and Navier-Stokes Equations", *Computers & Fluids*, Vol. 22 (2-3), pp. 259–270.

[8] Himeno, T., Watanabe, T., and Konno, A., 2005, "Numerical Analysis for Propellant Management in Rocket Tanks", *Journal of Propulsion and Power*, Vol. 21 (1), pp. 76–86.